ORIGINAL RESEARCH

Intracranial Dural Arteriovenous Fistula with Retrograde Cortical Venous Drainage: Use of Susceptibility-Weighted Imaging in Combination with Dynamic Susceptibility Contrast Imaging

K. Noguchi
N. Kuwayama
M. Kubo
Y. Kamisaki
K. Kameda
G. Tomizawa
H. Kawabe
H. Seto

EDITOR'S CHOICES

BACKGROUND AND PURPOSE: SWI is a new MR imaging method that maximizes sensitivity to magnetic susceptibility effects with phase information for visualizing small cerebral veins. The purpose of this study was to report the use of SWI in combination with DSC in examining related RCVD in patients with intracranial DAVFs.

MATERIALS AND METHODS: Ten patients with angiographically confirmed DAVFs with RCVD underwent conventional MR imaging, SWI, and DSC. The ability of SWI to depict dilated cerebral veins was evaluated and then compared with DSC. The hemispheres of patients with DAVFs were grouped into affected (with RCVD) or nonaffected (without RCVD) categories by angiography. Four patients had bilaterally affected hemispheres. A total of 14 affected hemispheres in patients with DAVFs with RCVD were evaluated.

RESULTS: SWI showed dilated cerebral veins on the surface of the brain in all (100%) of the 14 affected hemispheres in patients with DAVFs with RCVD and deep in the brain in 9 (64%). T2-weighted imaging showed prominent flow-voids on the surface of the brain in 10 (71%) of the 14 affected hemispheres in patients with DAVFs with RCVD and deep in the brain in 5 (36%). DSC showed increased cerebral blood volume in all of the 14 affected hemispheres. The SWI findings regarding dilated veins on the surface of the brain corresponded well with the areas of increased cerebral blood volume.

CONCLUSIONS: SWI in combination with DSC could be used to characterize the presence of RCVD in patients with DAVFs.

ABBREVIATIONS: CBV = cerebral blood volume; DAVF = dural arteriovenous fistula; DSC = dynamic susceptibility-weighted contrast-enhanced perfusion MR imaging; EPI = echo-planar imaging; GE = gradient-echo; MR-DSA = MR digital subtraction angiography; rCBV = relative cerebral blood volume; RCVD = retrograde cortical venous drainage; SSS = superior sagittal sinus; SWI = susceptibility-weighted imaging; TSS = transverse-sigmoid sinus; TS = torcular herophili

Intracranial DAVFs are grouped as benign or aggressive depending on the pattern of venous drainage revealed by angiography.[1-8] The classification schemes of Borden et al[4] and Cognard et al[5] are the most widely used. RCVD is the most significant risk factor associated with the more aggressive behavior of DAVFs.[3-8] DAVFs with RCVD can cause intraparenchymal or subarachnoid hemorrhage, parenchymal deficits, seizures, or dementia arising from venous hypertension due to impaired venous drainage.[7,8] Angiography is the most effective technique for diagnosing a DAVF. Findings of angiographic examinations reveal arteriovenous shunts, venous outflow obstruction, RCVD, and venous congestion. The angiographic appearance of brain parenchymal venous drainage is delayed, confirming widespread venous congestion.[9]

Conventional MR imaging findings are typically normal in patients with DAVFs without RCVD. In contrast, conventional MR imaging often shows prominent flow-voids on the surface of the brain in patients with DAVFs with RCVD and venous congestion.[9-12] Several investigators have previously reported that MR-DSA is a reliable technique for the screening and monitoring of DAVFs, despite its temporal- and spatial-resolution limitations, and that it clearly shows RCVD.[1-18] MR-DSA provides reliable information that can be used to determine the need for patients with DAVFs to undergo additional angiography.[16] A recent study reported that the increased cerebral blood volume in the affected hemisphere of patients with DAVFs with RCVD could be demonstrated with DSC because RCVD causes an increase in cerebral blood volume as a result of the dilation of cerebral veins.[19]

SWI is an imaging method that maximizes sensitivity to magnetic susceptibility effects. It is useful for the evaluation and detailed visualization of venous vessels and the depiction of hemorrhage.[20,21] SWI is already used for the imaging of trauma, tumors, multiple sclerosis, poststroke, and occult vascular disease and for the quantification of brain iron.[20-30] The purpose of this study was to report on the use of SWI in combination with DSC in examining related RCVD in patients with DAVFs.

Materials and Methods

Patients

A summary of patients with DAVFs with RCVD data is presented in the Table. Ten patients (5 men and 5 women; age range, 48–77 years; mean age, 64.4 years) with angiographically confirmed DAVFs with

Received February 25, 2010; accepted after revision May 20.

From the Departments of Radiology (K.N., Y.K., K.K., G.T., H.K., H.S.) and Neurosurgery (N.K., M.K.), Toyama University, Toyama, Japan.

Please address correspondence to Kyo Noguchi, MD, Department of Radiology, Toyama University, 2630 Sugitani, Toyama 930-0194, Japan; e-mail: kyo@med.u-toyama.ac.jp

DOI 10.3174/ajnr.A2231

Data of patients with DAVFs with RCVD

Case No.	Age (yr)/ Sex	Main Clinical Findings	Site of DAVF	Site of RCVD	Classification of DAVF	Increased CBV	Dilated Veins on SWI		Prominent Flow Void	
							Surface	Deep	Surface	Deep
1	48/F	Pulsatile tinnitus	Left TSS	Left	IIb	Yes	Yes	Yes	Yes	No
2	73/F	Pulsatile tinnitus	Left TSS	Left	IIb	Yes	Yes	No	No	No
3	77/M	Headache	SSS	Both	IIb	Yes, both	Yes, both	Yes, both	Yes, both	No
4	60/M	Papilledema	TS	Both	IIa + b	Yes, both	Yes, both	Yes, both	Yes, both	Yes, both
5	74/F	Hemorrhage	Left TSS	Left	IIb	Yes	Yes	No	No	No
6	62/M	Dementia	Right TSS	Right	IIa + b	Yes	Yes	Yes	Yes	Yes
7	77/F	Dementia	Right TSS	Both	IIa + b	Yes, both	Yes, both	Yes, left	No	No
8	57/F	Hemorrhage	SSS	Both	IIb	Yes, both	Yes, both	Yes, both	Yes, both	Yes, both
9	67/M	Hemorrhage	Right TSS	Right	IIb	Yes	Yes	No	Yes	No
10	55/M	Headache	Right TSS	Right	III	Yes	Yes	No	Yes	No

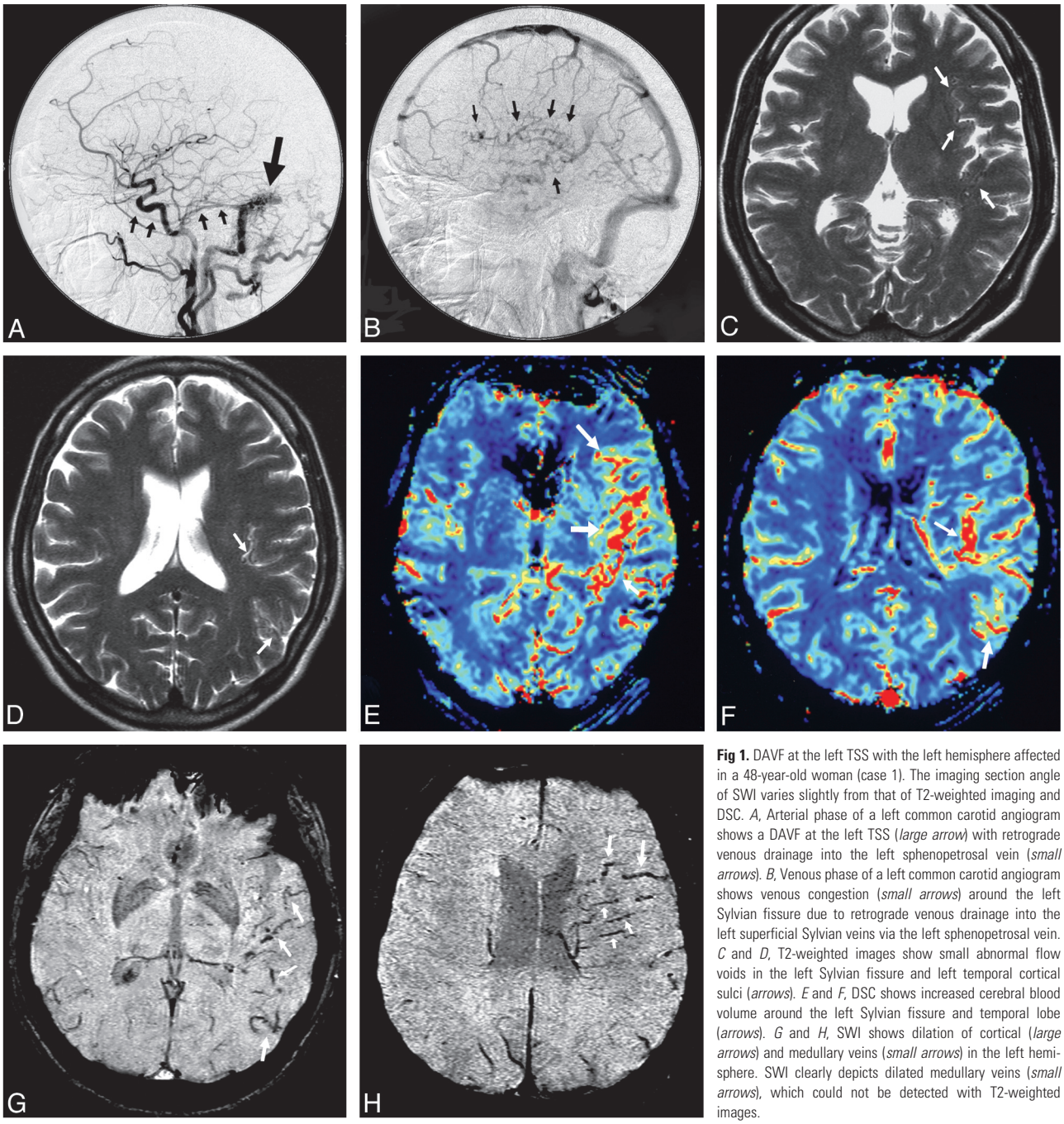

Fig 1. DAVF at the left TSS with the left hemisphere affected in a 48-year-old woman (case 1). The imaging section angle of SWI varies slightly from that of T2-weighted imaging and DSC. *A,* Arterial phase of a left common carotid angiogram shows a DAVF at the left TSS (*large arrow*) with retrograde venous drainage into the left sphenopetrosal vein (*small arrows*). *B,* Venous phase of a left common carotid angiogram shows venous congestion (*small arrows*) around the left Sylvian fissure due to retrograde venous drainage into the left superficial Sylvian veins via the left sphenopetrosal vein. *C* and *D,* T2-weighted images show small abnormal flow voids in the left Sylvian fissure and left temporal cortical sulci (*arrows*). *E* and *F,* DSC shows increased cerebral blood volume around the left Sylvian fissure and temporal lobe (*arrows*). *G* and *H,* SWI shows dilation of cortical (*large arrows*) and medullary veins (*small arrows*) in the left hemisphere. SWI clearly depicts dilated medullary veins (*small arrows*), which could not be detected with T2-weighted images.

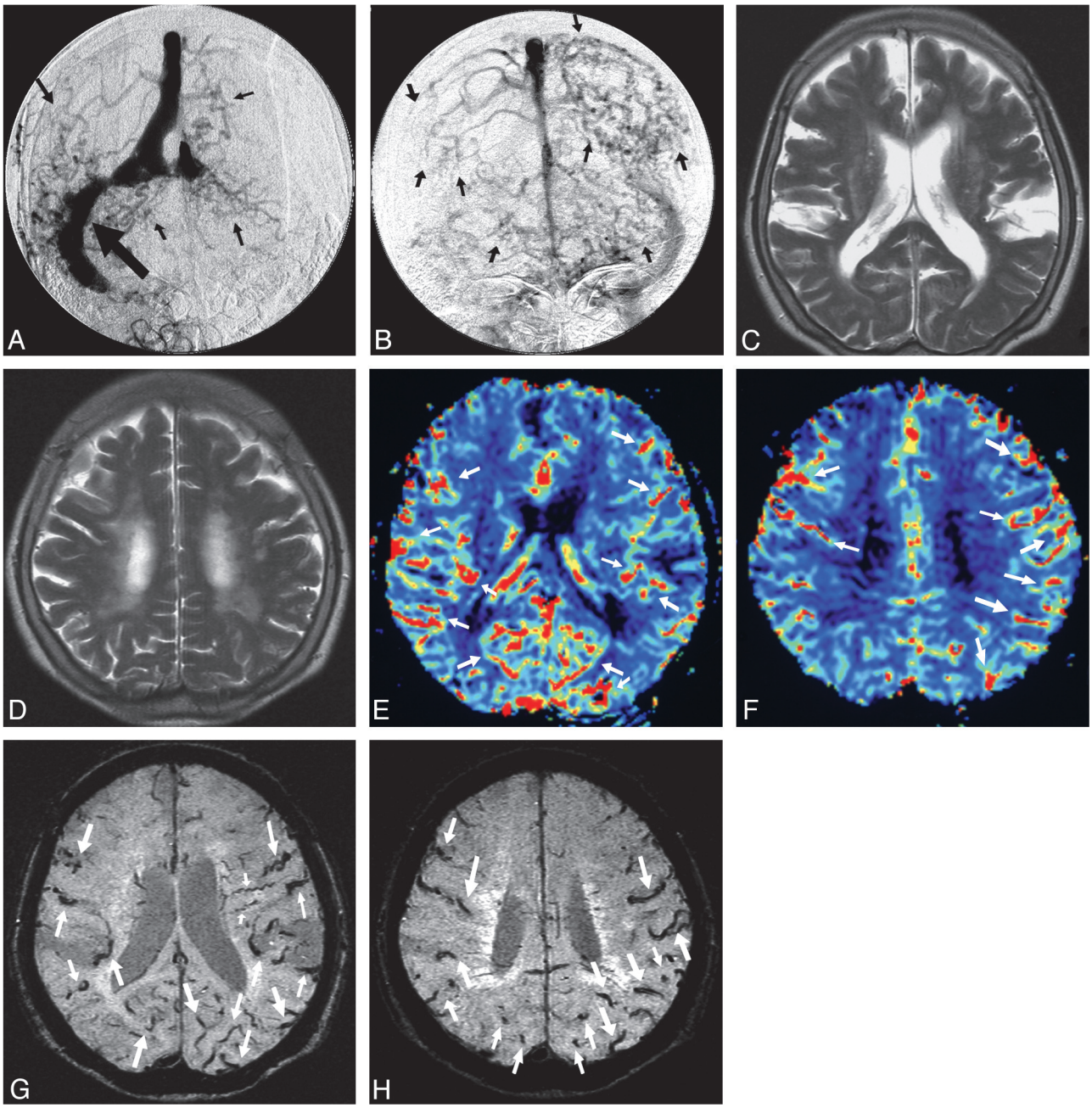

Fig 2. DAVF at the right TSS with both hemispheres affected in a 77-year-old woman (case 7). *A,* Arterial phase of a right external carotid angiogram shows a DAVF at the right TSS (*large arrow*) with retrograde venous drainage into the superior sagittal sinus and bilateral cortical veins (*small arrows*), with occlusions of the distal portion of right sigmoid sinus and of the proximal portion of left transverse sinus. *B,* Venous phase of a right external carotid angiogram shows marked venous congestion (*arrows*) in both hemispheres. *C* and *D,* T2-weighted image shows no abnormal flow-voids. *E* and *F,* DSC shows increased cerebral blood volume in both hemispheres (*arrows*). *G* and *H,* SWI shows dilation of cortical veins (*large arrows*) in both hemispheres and dilation of medullary veins (*small arrows*) in the left hemisphere.

RCVD were studied. Patients underwent T1- and T2-weighted imaging, DSC, and SWI. In addition, 3 patients (2 men and 1 woman; age range, 49–75 years; mean age, 58 years) with angiographically confirmed DAVFs without RCVD underwent T1- and T2-weighted imaging and SWI. Informed consent was obtained from all patients.

MR Imaging

MR imaging was performed with a 1.5T superconducting unit (Magnetom Vision; Siemens, Erlangen, Germany) with a standard head coil. Routine T1-weighted spin-echo and T2-weighted turbo spin-echo imaging was performed. TR was 550 and 5000 ms, and TE was 15 and 90 ms, for T1- and T2-weighted imaging, respectively. All images were obtained with a 22-cm FOV and a 192 × 256 matrix. Section thickness was 7 mm.

DSC

DSC was performed with GE-type EPI. The imaging parameters were as follows: TR, 1000 ms; TE, 60.7 ms; flip angle, 60°; FOV, 24 cm; matrix, 128 × 128; section thickness, 7 mm; acquisitions, 1. A bolus injection of 0.1 mmol/kg of gadolinium-based contrast agent at 3 mL/s was immediately followed by a bolus injection of saline (total of 20 mL at the same rate) by power injector, and each section was sampled 60 times a minute. DSC covered the section through the basal ganglia to the body of the lateral ventricle in 5 sections. To create

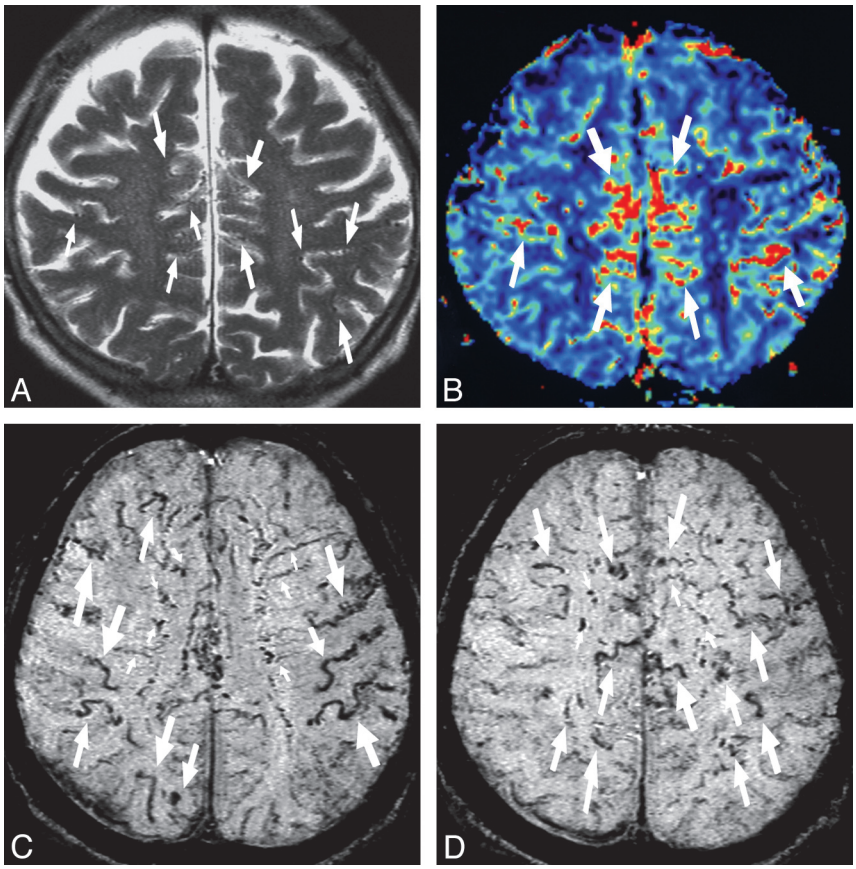

Fig 3. DAVF at the superior sagittal sinus with both hemispheres affected in a 77-year-old man (case 3). *A,* T2-weighted image shows multiple abnormal small flow-voids (*arrows*) in the interhemispheric fissures. *B,* DSC shows increased cerebral blood volume around the interhemispheric fissures and parietal sulci (*arrows*). *C* and *D,* SWI shows dilation of cortical (*large arrows*) and medullary veins (*small arrows*) in both hemispheres.

a qualitative rCBV map, we first converted the measured time-signal-intensity curves into a time-concentration curve and then fitted it with a γ variate function to eliminate recirculation effects. Blood volume values were determined by using equations obtained from the indicator dilution theory by calculating the area under the tissue time-concentration curve on a pixel-by-pixel basis.

SWI

SWI was performed according to a previously described technique.[20,22] This sequence consisted of a strongly T2*-weighted low-bandwidth 3D fast low-angle shot sequence, with flow compensated in all 3 orthogonal directions. The detailed imaging parameters were as follows: TR, 57 ms; TE, 40 ms; and flip angle, 20°. Thirty-two partitions of 2 mm were acquired by using a rectangular FOV (5/8) of 256 mm and a matrix size of 160 × 512, resulting in a voxel size of 1 × 0.5 × 2 mm^3. The acquisition time was 4 minutes 47 seconds. SWI images were created by using the magnitude and phase raw datasets. A phase mask was created by setting all positive phase values (between 1° and 180°) to unity and by normalizing the negative phase values ranging from 0° to −180° to a gray-scale of values ranging linearly from unity to zero, respectively. This normalized phase mask was multiplied 4 times against the original magnitude image and yielded images that enhanced the hypointensities of the region containing susceptibility properties (such as deoxygenated venous blood, clots, and hemosiderin). Last, a minimum intensity projection over 2 sections was performed to display the processed data by using contiguous sections of 4-mm thickness in the axial plane. The processing was automatically performed by the Magnetom Vision software (Siemens).

Image Interpretation

The T2-weighted images, SWI, and DSC (rCBV map) were independently reviewed by 2 neuroradiologists, who had no background knowledge of patient clinical data or angiography findings. Disagreements were resolved by consensus. The ability of each T2-weighted image and SWI to depict prominent cerebral veins was evaluated, and SWI was compared with DSC.

Results

A summary of patient data is presented in the Table. Three of the patients had subcortical hemorrhages, 2 of these 3 patients had white matter edema, and 2 of the remaining patients had dementia. The hemispheres of patients with DAVFs with RCVD were grouped into affected (the hemisphere with RCVD) or nonaffected (the hemisphere without RCVD) categories, depending on the presence or absence of RCVD as revealed by angiography. Four patients with DAVFs had bilaterally affected hemispheres. A total of 14 affected hemispheres and 6 nonaffected hemispheres in patients with DAVFs with RCVD were evaluated.

SWI revealed dilated cerebral veins on the surface of the brain in all (100%) of the 14 affected hemispheres in patients with DAVFs with RCVD and deep in the brain in 9 (64%) of the 14 affected hemispheres in patients with DAVFs with RCVD (Figs 1–3). T2-weighted imaging showed prominent flow-voids on the surface of the brain in 10 (71%) of the 14 affected hemispheres in patients with DAVFs with RCVD and deep in the brain in 5 (36%) of the 14 affected hemispheres in patients with DAVFs with RCVD. In all patients with DAVFs

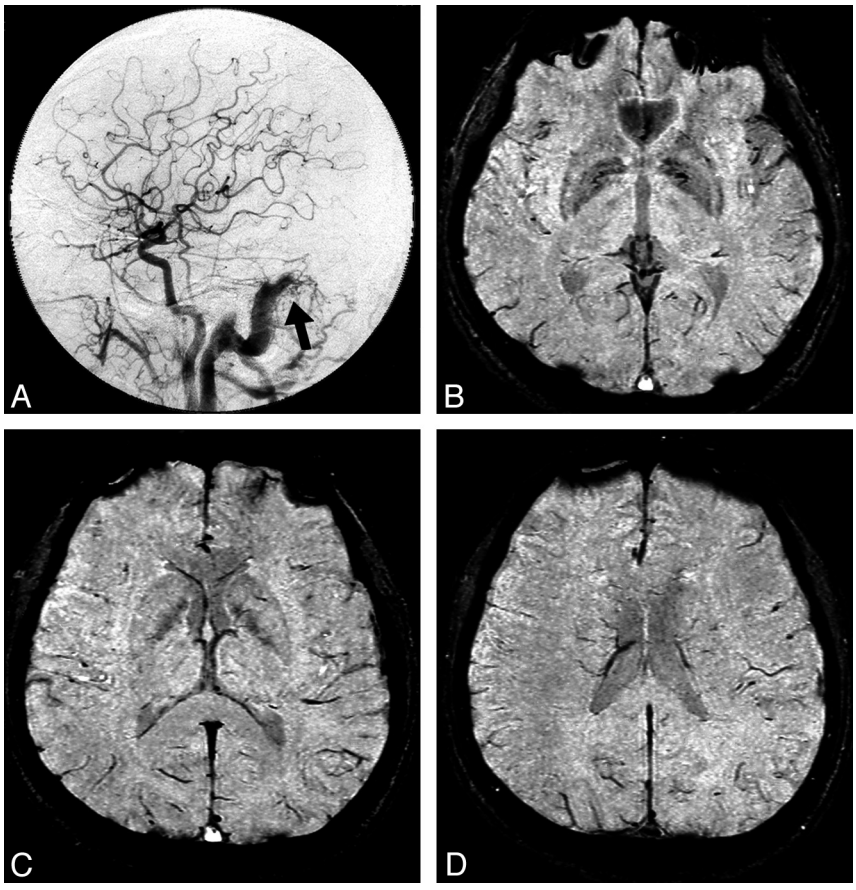

Fig 4. DAVF at the right TSS without RCVD in a 50-year-old man. *A,* Arterial phase of a right common carotid angiogram shows a DAVF at the right TSS (*arrow*) without RCVD. *B—D,* SWI shows no dilated cerebral veins.

with RCVD, DSC showed increased cerebral blood volume in all of the 14 affected hemispheres. The SWI findings of dilated veins on the surface corresponded well with the areas of increased cerebral blood volume. In all 6 nonaffected hemispheres of patients with DAVFs with RCVD, SWI did not indicate dilated cerebral veins and DSC showed no increased cerebral blood volume. In all 3 patients with DAVFs without RCVD, SWI did not show dilated cerebral veins (Fig 4).

In 1 patient with DAVF with large and small subcortical hemorrhages in the right temporo-occipital region, it was difficult to differentiate dilated veins and small hemorrhages by using SWI alone (Fig 5). In another patient with a DAVF with venous drainage directly into the vein of Labbé (Cognard classification type III), SWI depicted a portion of dilated cerebral veins as hyperintense (Fig 6).

Discussion

SWI clearly showed dilated cerebral veins, indicating venous drainage impairment in patients with DAVFs with RCVD. SWI uses a fully velocity-compensated high-resolution 3D-GE sequence that uses magnitude and filtered-phase information.[20,22] It was originally referred to as high-resolution blood oxygenation level—dependent venography.[20] SWI permits extremely sensitive analysis of venous vasculature and hemorrhages.[20,26,27] During the past decade, SWI has been found to provide additional clinically useful information that is often complementary to conventional MR imaging sequences used in the evaluation of various neurologic disorders, including traumatic brain injury, other hemorrhagic disorders, vascular malformations, infarctions, tumors, and neurodegenerative disorders associated with intracranial calcification or iron deposition.[20-29] SWI is also useful in multiple sclerosis imaging.[30] These lesions might be better characterized with MR imaging by using an SWI sequence.

Lee et al[29] studied 10 patients and concluded that SWI is ideal for screening patients with a high clinical suspicion of low-flow vascular malformations such as cavernomas. Reichenbach et al[21] also reported a similar result for a developmental venous anomaly. Saini et al[31] reported a patient with a DAVF with delayed cerebral venous drainage, which was imaged with SWI in addition to conventional MR imaging, and suggested that the use of SWI might be helpful in the early diagnosis of DAVFs. Our study showed that SWI was superior to T2-weighted imaging in the detection of dilated veins (medullary veins) deep in the brain, probably because small and/or very slow-flowing veins may not be detected with T2-weighted images. SWI clearly showed small and very slow-flowing veins because of its increased spatial resolution and strong susceptibility contrast. We believe that SWI is more sensitive than T2-weighted imaging for dilated medullary veins.

Our study revealed that DSC was extremely sensitive at revealing the dilated cortical veins indicating RCVD in patients with DAVFs. DSC was performed by using GE-type EPI in this study. DSC with GE is more sensitive than spin-echo sequences for flow in larger caliber vessels. Although the greater susceptibility effect created in and around larger ves-

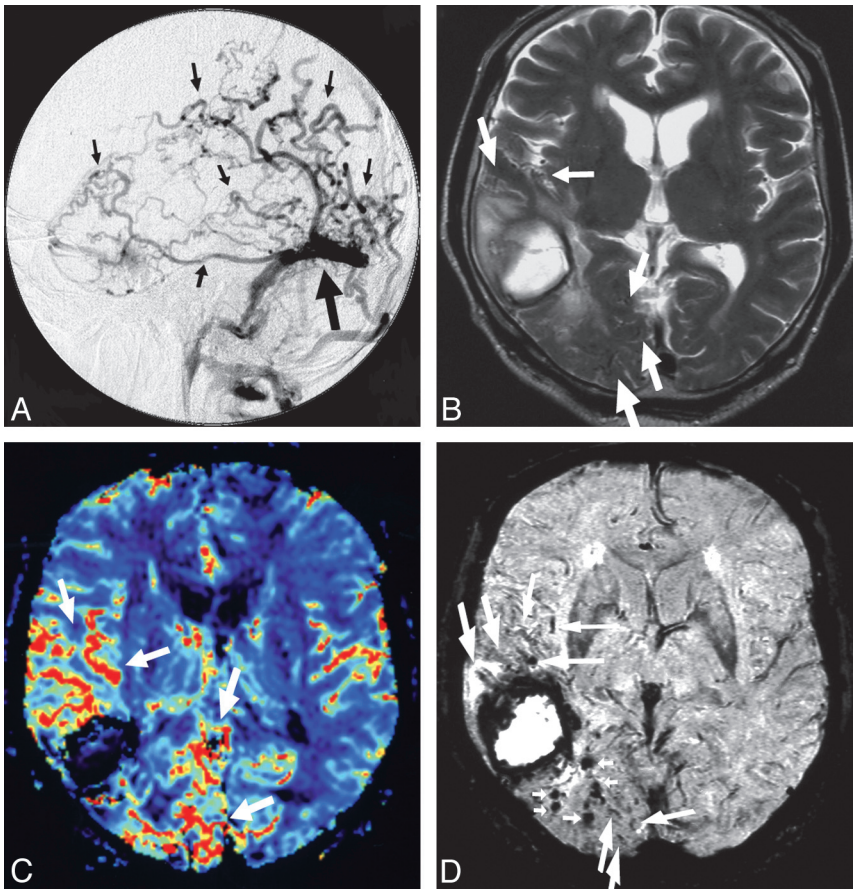

Fig 5. DAVF at the right TSS with the right hemisphere affected in a 67-year-old man (case 9). *A,* Arterial phase of a right external carotid angiogram shows a DAVF at the right TSS (*large arrow*) with RCVD in the right hemisphere (*small arrows*). *B,* T2-weighted image shows a subcortical hematoma in the right temporal lobe and abnormal flow voids around the hematoma in the right temporo-occipital region (*arrows*). *C,* DSC shows increased cerebral blood volume around the hematoma in the right temporal and occipital lobes (*arrows*). *D,* SWI shows dilation of cerebral veins (*large arrows*) and large and small hemorrhages (*small arrows*) in the right temporo-occipital region. Although it is difficult to definitively discriminate dilated venous structures and small hematomas by using SWI alone, the combination of DSC and SWI overcomes this limitation.

sels with GE sequences may lead to overestimation of cerebral blood volume in these lesions, contrast-to-noise ratios are greater in GE sequences than in SE sequences. Our study suggested that the combination of SWI and DSC provided a very sensitive approach for the evaluation of RCVD in patients with DAVF.

Angiography should be performed to confirm the diagnosis of a DAVF. Angiography clearly shows evidence of arteriovenous shunts, venous outflow obstruction, and RCVD. RCVD with venous congestion is depicted as dilated and tortuous veins as well as focal regions of delayed circulation in the late venous phase of angiography.[9] It is often difficult, however, to evaluate hemodynamics objectively on the basis of angiographic findings in patients with DAVFs with RCVD because the angiographic findings of DAVF are complex, consisting of combinations of arteriovenous shunts, RCVD, sinus occlusions, and impaired parenchymal circulation. As such, additional cross-sectional imaging techniques are required to achieve more accurate evaluation of venous drainage impairment in patients with DAVFs with RCVD.

Conventional MR imaging findings are typically normal in patients with DAVFs without RCVD. Conventional MR imaging, however, often shows prominent flow voids on the surface of the brain in patients with DAVFs with RCVD.[9-12] High-intensity lesions in the deep white matter revealed by T2-weighted imaging are secondary to the venous hypertension and venous congestion. The combination of prominent flow voids on the surface of the brain and high intensity lesions in T2-weighted images within the deep white matter is highly suggestive of a DAVF.[12] The demonstration of medullary vein enlargement on MR images may be a key marker of venous congestion due to venous-outflow obstruction.

Our study has some important limitations. First, it is difficult for SWI to differentiate small venous structures from small hemorrhages because the signal-intensity characteristics are similar (case 9, Fig 5). Susceptibility effects sometimes made it difficult to differentiate small veins and small hemorrhages. The combination of SWI and DSC or conventional MR imaging, however, can mitigate this disadvantage.

Second, SWI is incapable of showing all dilated cortical veins depicted as typical hypointense vessels in a patient with a DAVF with venous drainage directly into a cortical vein (Cognard classification type III). SWI depicts a portion of dilated cerebral veins as hyperintense vessels (case 10, Fig 6). Magnetic field inhomogeneity due to paramagnetic deoxygenated venous blood results in a reduction of T2* and a phase difference between the vessel and its surroundings.[32,33] At 1.5T, arterial blood has a T2* of approximately 200 ms, while 70% saturated venous blood has a T2* of approximately 100 ms.[21] Accordingly, SWI allows the differentiation of arteries from

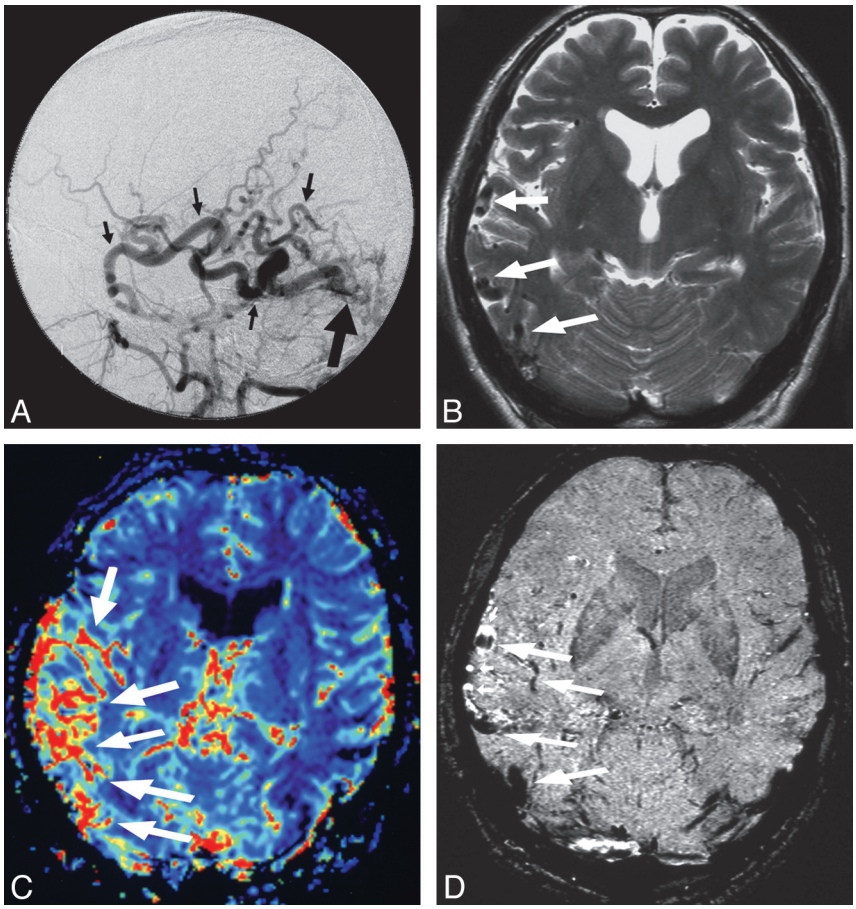

Fig 6. DAVF at the right TSS with a right affected hemisphere in a 55-year-old man (case 10). *A,* Arterial phase of a right external carotid angiogram shows a DAVF (*large arrow*) with venous drainage directly into the right vein of Labbé (Cognard classification type III) (*arrows*). *B,* T2-weighted image shows abnormal flow voids in the right temporo-occipital region (*arrows*). *C,* DSC shows increased cerebral blood volume in the right temporo-occipital region (*arrows*). *D,* SWI depicts dilated cerebral veins as hyperintense vessels (*small arrows*), though most dilated cortical veins are seen as typical hypointense vessels (*large arrows*).

veins because the deoxyhemoglobin behaves like a contrast agent in the visualization of venous structures. SWI cannot show nondeoxygenated (oxygenated) RCVD depicted as typical hypointense veins because that arterial blood drains directly into cortical veins (Cognard classification type III). The combination of SWI and other MR images, such as DSC or conventional MR imaging, however, can mitigate this disadvantage.

Third, the number of patients with DAVFs with RCVD was limited. Further studies with larger subject groups, including patients with DAVFs with variable degrees of RCVD and treated patients, would be required to fully assess this technique. Fourth, the imaging section angle of SWI varied slightly from that of other MR images in 2 of the cases.

Conclusions

In this study, DSC was extremely sensitive at revealing dilated cortical veins and SWI could more clearly show dilated medullary veins than conventional MR imaging. SWI in combination with DSC could thus be used to characterize the presence of RCVD in patients with DAVFs.

References

1. Awad I, Little J, Akrawi W, et al. **Intracranial dural arteriovenous malformations: factors predisposing to an aggressive neurological course.** *J Neurosurg* 1990;72:839–50
2. Malik GM, Pearce JE, Ausman JI, et al. **Dural arteriovenous malformations and intracranial hemorrhage.** *Neurosurgery* 1984;15:332–39
3. Vinuela F, Fox AJ, Pelz DM, et al. **Unusual clinical manifestations of dural arteriovenous malformations.** *J Neurosurg* 1986;64:554–58
4. Borden JA, Wu JK, Shucart WA. **A proposed classification for spinal and cranial dural arteriovenous fistulous malformations and implications for treatment.** *J Neurosurg* 1995;82:166–79
5. Cognard C, Gobin Y, Pierot L, et al. **Cerebral dural arteriovenous fistulas: clinical and angiographic correlation with a revised classification of venous drainage.** *Radiology* 1995;194:671–80
6. van Dijk JM, terBrugge KG, Willinsky RA, et al. **Clinical course of cranial dural arteriovenous fistulas with long-term persistent cortical venous reflux.** *Stroke* 2002;33:1233–36
7. Lasjaunias P, Chiu M, terBrugge K, et al. **Neurological manifestations of intracranial dural arteriovenous malformations.** *J Neurosurg* 1986;64:724–30
8. Hurst RW, Bagley LJ, Galetta S, et al. **Dementia resulting from dural arteriovenous fistulas: the pathologic findings of venous hypertensive encephalopathy.** *AJNR Am J Neuroradiol* 1998;19:1267–73
9. Willinsky R, Goyal M, terBrugge K, et al. **Tortuous, enlarged pial veins in intracranial dural arteriovenous fistulas: correlations with presentation, location, and MR findings in 122 patients.** *AJNR Am J Neuroradiol* 1999;20:1031–36
10. DeMarco K, Dillon WP, Halbach VV, et al. **Dural arteriovenous fistula: evaluation with MR imaging.** *Radiology* 1990;175:193–99
11. Chen JC, Tsuruda JS, Halbach VV. **Suspected dural arteriovenous fistula: results with screening MR angiography in seven patients.** *Radiology* 1992;183:265–71
12. Willinsky R, terBrugge K, Montanera W, et al. **Venous congestion: an MR finding in dural arteriovenous malformations with cortical venous drainage.** *AJNR Am J Neuroradiol* 1994;15:1501–07
13. Noguchi K, Melhem ER, Kanazawa T, et al. **Intracranial dural arteriovenous fistulas: evaluation with combined 3D time-of-flight MR angiography and MR digital subtraction angiography.** *AJR Am J Roentgenol* 2004;182:183–90
14. Coley SC, Romanowski CA, Hodgson TJ, et al. **Dural arteriovenous fistulae:**

noninvasive diagnosis with dynamic MR digital subtraction angiography. *AJNR Am J Neuroradiol* 2002;23:404–07
15. Horie N, Morikawa M, Kitigawa N, et al. **2D thick-section MR digital subtraction angiography for the assessment of dural arteriovenous fistulas.** *AJNR Am J Neuroradiol* 2006;27:264–69
16. Noguchi K, Kuwayama N, Kubo M, et al. **Dural arteriovenous fistula involving the transverse sigmoid sinus after treatment: assessment with magnetic resonance digital subtraction angiography.** *Neuroradiology* 2007;49:639–43
17. Farb RI, Agid R, Willinsky RA, et al. **Cranial dural arteriovenous fistula: diagnosis and classification with time-resolved MR angiography at 3T.** *AJNR Am J Neuroradiol* 2009;30:1546–51
18. Nishimura S, Hirai T, Sasao A, et al. **Evaluation of dural arteriovenous fistulas with 4D contrast-enhanced MR angiography at 3T.** *AJNR Am J Neuroradiol* 2010;31:80–85
19. Noguchi K, Kubo M, Kuwayama N, et al. **Intracranial dural arteriovenous fistulas with retrograde cortical venous drainage: assessment with cerebral blood volume by dynamic susceptibility contrast magnetic resonance imaging.** *AJNR Am J Neuroradiol* 2006;27:1252–56
20. Reichenbach JR, Venkatesan R, Schillinger DJ, et al. **Small vessels in the human brain: MR venography with deoxyhemoglobin as an intrinsic contrast agent.** *Radiology* 1997;204:272–77
21. Reichenbach JR, Jonetz-Mentzel L, Fitzek C, et al. **High-resolution blood oxygen-level dependent MR venography.** *Neuroradiology* 2001;43:364–69
22. Haacke EM, Xu Y, Cheng YC, et al. **Susceptibility-weighted imaging (SWI).** *Magn Reson Med* 2004;52:612–18
23. Barth M, Nobauer-Huhmann IM, Reichenbach JR, et al. **High-resolution three-dimensional contrast-enhanced blood oxygenation level-dependent magnetic resonance venography of brain tumors at 3 Tesla: first clinical experience and comparison with 1.5 Tesla.** *Invest Radiol* 2003;38:409–14
24. Haacke EM, Herigault G, Kido D, et al. **Observing tumor vascularity noninvasively using magnetic resonance imaging.** *Image Anal Stereol* 2002;21:107–13
25. Wycliffe ND, Choe J, Holshouser B, et al. **Reliability in detection of hemorrhage in acute stroke by a new three-dimensional gradient recalled echo susceptibility-weighted imaging technique compared to computed tomography: a retrospective study.** *J Magn Reson Imaging* 2004;20:372–77
26. Tong KA, Ashwal S, Holshouser BA, et al. **Hemorrhagic shearing lesions in children and adolescents with posttraumatic diffuse axonal injury: improved detection and initial results.** *Radiology* 2003;227:332–39
27. Tong KA, Ashwal S, Holshouser BA, et al. **Diffuse axonal injury in children: clinical correlation with hemorrhagic lesions.** *Ann Neurol* 2004;56:36–50
28. Ogg RJ, Langston JW, Haacke EM, et al. **The correlation between phase shifts in gradient-echo MR images and regional brain iron concentration.** *Magn Reson Imaging* 1999;17:1141–48
29. Lee BC, Vo KD, Kido DK, et al. **MR high-resolution blood oxygenation level–dependent venography of occult (low-flow) vascular lesions.** *AJNR Am J Neuroradiology* 1999;20:1239–42
30. Haacke EM, Makki M, Ge Y, et al. **Characterizing iron deposition in multiple sclerosis lesions using susceptibility weighted imaging.** *J Magn Reson Imaging* 2009;29:537–44
31. Saini J, Thomas B, Bodhey NK, et al. **Susceptibility-weighted imaging in cranial dural arteriovenous fistulas.** *AJNR Am J Neuroradiol* 2009;30:E6
32. Thulborn KR, Waterton JC, Matthews PM, et al. **Oxygenation dependence of the transverse relaxation time of water protons in whole blood at high field.** *Biochim Biophys Acta* 1982;714:265–70
33. Li D, Waight DJ, Wang Y. **In vivo correlation between blood T2* and oxygen saturation.** *J Magn Reson Imaging* 1998;8:1236–39